Substitutional and vacancy defects in two-dimensional AlSb: A first principle approach

A thesis presented to the Department of Materials Science and Engineering
African University of Science and Technology, Abuja
in partial fulfilment of the requirements for the award of

Master of Science Degree

By

UDOFIA Benjamin Etim

Supervised by

Dr. Emmanuel Igumbor

African University of Science and Technology
www.aust.edu.ng
P.M.B 681, Garki, Abuja F.C.T
Nigeria.

July, 2019

Substitutional and vacancy defects in two-dimensional AlSb: A first principle approach

By

UDOFIA Benjamin Etim

A thesis approved by the Department of Materials Science and Engineering

Recommended:

.....

Supervisor: Dr. Emmanuel Igumbor

.....

Co-Supervisor: Dr. Abdulhakeem Bello

.....

Head, Department of Materials Science and Engineering

APPROVED:

.....

Chief Academic Officer (Prof. C. E. Chidume)

.....

Date

Abstract

AlSb is a semiconductor material which exist in 3D as well as 2D regimes. AlSb have a high electron mobility which is useful for application in high speed electronic devices. AlSb has potential applications in radiation detection. Defects, including intrinsic and extrinsic have been shown to influence the performance of AlSb for applications in electronic and optoelectronics. In this thesis, density functional theory with the aid of the generalised gradient approximation was use to model the stability as well as the formation of Al and Sb vacancies, Li and Be substitutions in 2D hexagonal AlSb. The structural and electronic properties of the aforementioned defects in AlSb were reported. Under equilibrium conditions, the aluminium vacancy (V_{Al}) is energetically more favourable than the antimony vacancy (V_{Sb}). While the Be substitution is more stable at the Al atomic site, the Li substitution is more stable at the Sb atomic site. The defects investigated modulated the band gap of the AlSb. Whereas the p orbital of the Sb atom contributed the dominant states in the band gap of the host for all the defects, the p orbital of Al contributed immensely to the defects states. The results further shows that using the generalised gradient approximation predicts defective AlSb as well as the pristine AlSb to be metallic. This has paved the way for further investigation using more accurate exchange correlation approximations.

Acknowledgements

My special appreciation goes to everyone who has contributed towards making this work a success!

- To my supervisors, **Dr. Emmanuel Igumbor** of University of South Africa and **Dr. Abdulhakeem Bello** of African University of Science and Technology, Abuja, I say a very big thank you! Your teachings and supervision immensely contributed to the success of this work.
- My friends and colleagues at African University of Science and Technology, I appreciate you all for the help and encouragement.
- To my beloved parents and siblings, I appreciate your financial, moral and spiritual supports throughout this period of my academic pursuit.
- To African University of Science and Technology, Department of Materials Science and Engineering, and all its sponsors, I say a big thank you.

Dedication

This project is dedicated to the Almighty God
who aided me intellectually and physically throughout the period of this project,
and to all the scientists that keep working to make the world a better place.

Contents

Abstract i

Acknowledgements ii

Dedication iii

Table of Contents vi

List of Abbreviation vii

List of Figures viii

List of Tables ix

1 Introduction 1

1.1 Background 1

1.2 Motivation and problem statement 2

1.3 Objectives 2

1.4 Overview and synopsis 3

2 Electronic structure methods and calculations 4

2.1 Variational principle 4

2.2 Many-body Hamiltonian 4

2.3 Born-Oppenheimer approximation 6

2.4 Hartree approximation 8

2.4.1 Hartree-Fock approximation 9

2.5 Density functional theory 12

2.5.1 Hohenberg-Kohn formalism 13

2.5.2 The Kohn-Sham equations 14

2.6 Exchange-correlation functionals 16

2.6.1 The local density approximation . . . 17
2.6.2 The generalized gradient approximation . . . 17
2.6.3 Hybrid functionals . . . 18
2.7 Pseudopotential . . . 19
2.7.1 Norm-conserving pseudopotentials . . . 20
2.7.2 Ultra-soft pseudopotentials . . . 20
2.7.3 The projector-augmented wave method . . . 21
2.8 Basis set . . . 21
2.9 Brillouin zone . . . 21

3 Literature review **23**
3.1 Defects in material . . . 23
3.1.1 Surface defects . . . 23
3.1.2 Line defects (dislocations) . . . 24
3.1.3 Point defect . . . 25
3.2 Defects in AlSb and other alloys . . . 26

4 Methodology **30**
4.1 Computational details . . . 30
4.2 Test of supercell size . . . 30
4.3 Test of cut-off energy . . . 31
4.4 Test of k-points . . . 32
4.5 Calculation details . . . 33

5 Results **34**
5.1 Structural properties . . . 34
5.2 Stability and energetics of defects . . . 36
5.3 Electronic properties . . . 37

6 Conclusions **39**
6.1 Summary . . . 39
6.2 Recommendation . . . 39

Bibliography **41**

List of Abbreviation

Born–Oppenheimer approximation	BOA
Brillouin zone	BZ
Density functional theory	DFT
Density of states	DOS
Exchange–correlation	E_{xc}
Generalized gradient approximation	GGA
Hartree approximation	HA
Hohenberg–Kohn	HK
Kohn–Sham	KS
Local density approximation	LDA
Monkhorst–Pack	MP
Projected–augmented wave	PAW
Projected density of states	PDOS
Self consistent field	SCF
Total density of states	TDOS
Two dimension	2D

List of Figures

2.1 A schematic flow chart illustrating the self consistent field calculation of the DFT [47]. 16

3.1 Grain boundaries [51]. 24
3.2 Mixed dislocation [49]. 25
3.3 Point defects in crystalline lattices [51]. 26

4.1 Plot of formation energy as a function of supercell for Al vacancy of AlSb. Here, the chemical potential was not taken into consideration since all the supercell required the same chemical potential. 31
4.2 Plot showing the total energy as a function of the E_{cut} as a test of convergence. 32
4.3 Convergence of total minimum energy of AlSb as a function of k-points sampling. (Kinetic energy cut-off of 45 Ry was used for the calculation). . 32

5.1 Fully relaxed geometric structures of (a) pristine; (b) Be impurity at the Al site; (c) Be impurity at the Sb site; (d) Li impurity at the Al site; (e) Li impurity at the Sb site; (f) Al vacancy and (g) Sb vacancy. 34
5.2 The TDOS and PDOS plots of (a) pristine; (b) Be impurity at the Al site; (c) Be impurity at the Sb site; (d) Li impurity at the Al site; (e) Li impurity at the Sb site; (f) Al vacancy and (g) Sb vacancy. The Fermi level is set to 0 eV. 37

List of Tables

5.1 The unrelax (UR) and relaxed (R) bond length in Å of atoms of defective AlSb. The relaxed pristine Al–Sb bond length (PR) is 2.686 Å. 35

5.2 The energy of formation E_{form} (eV) of vacancy and substitutional impurities in AlSb. 36

CHAPTER 1

Introduction

This chapter presents a brief introduction of the topic of interest – substitutional and vacancy defects in two-dimensional hexagonal AlSb. The motivation of the study, the objectives and synopsis of the thesis are presented in this chapter.

1.1 Background

Properties of high-pressure materials including AlSb, AlSi, CdTe, C-BN, C-BC_2N, TiB_2, SiC, TiN, amongst others ranges from superconducting behaviour to super hard properties, high density, highly incompressible, high thermal conductivity, non-linear optical properties (frequency-doubling) and unusual electronic and magnetic properties. These unique properties can be utilized for applications in semiconductor diodes and lasers [1], energy storage materials [2], high-temperature electronics and optoelectronics applications [3]. In recent years, two dimension (2D) materials such as graphene, phosphorene, transition metal dichalcogenides, boron nitride (BN) in their monolayer regime, have the potentials to enhance existing technologies and also create a range of new applications for future opto-electronic nano-devices, because of the extraordinary electrical, mechanical and optical properties they possess [4]. 2D AlSb is of considerable research and technical interest because of its many features like monolayer materials. It has a direct and indirect energy gap of 1.62 eV and 1.31 eV respectively coupled with a unique band alignment [5]. In the past, AlSb has been utilized in opto-electronic devices [6], radiation detection [7], application for lithium-ion and sodium-ion storage [8], and as buffer layer for the epitaxial growth of GaSb [9].

1.2 Motivation and problem statement

Technological advancement in electronics have progressed astronomically in the past decade, transforming from basic electronics to revolutionary high speed electronics. The understanding of defects and how they influence this new technology is limited. Defects is known to influence the performance of several 2D materials. For example, deep defects in SiC and diamond have been courted for application in quantum information. Several studies of defects in 2D materials have been reported [10, 11, 12] however, for 2D AlSb, there are few studies of defects reported [13, 14, 15]. Optoelectronics play a major role in the semiconductor industry, and silicon-based optoelectronics are presently so prevalent in current society. scaling down and improving the performance of current silicon-based devices are still very challenging. Therefore, new materials have to be developed to meet these challenges. AlSb has the potential to be engineered for specific applications due to its unique properties. 2D AlSb has a high electron mobility and is a candidate for high speed electronics, solar cells and photo-detectors. One of the major challenges of utilising the AlSb, is the presence of point defects during fabrication and synthesis. Point defects may be created in AlSb via experimental techniques (including electron irradiation, electron bean exposure, molecular vapour deposition, ion implantation) and hence could influence its performance in device application. For example, the activities of point defects such as vacancies, interstitials, substitutions and their complexes as they affects the electronic, optical and structural properties of AlSb are not fully understood.

1.3 Objectives

This work is aimed at studying the stability, electronic properties and formation of defects in 2D hexagonal AlSb. The Sb vacancy (V_{Sb}), Al vacancy (V_{Al}), Li substituted for Sb (Li_{Sb}) and Al (Li_{Al}) and Be substituted for Sb (Be_{Sb}) and Al (Be_{Al}) atoms were studied. The computational prediction was performed from first principles calculations via density functional theory (DFT) with the generalized gradient approximation (GGA).

1.4 Overview and synopsis

In this thesis, we have used DFT to model the substitutional and vacancy defects in 2D AlSb. The Li and Be are the external dopants introduced in AlSb in addition to Al and Sb vacancies. The thesis is organized as follows:

- **Chapter 1** gives a general introduction of the thesis with emphasis on 2D materials and their potential applications.
- **Chapter 2** discussion of the electronic structure methods and calculations used for this study are presented.
- **Chapter 3** provides a short review of defects in semiconductor. A compressive review of first-principles studies of doping and defects in binary high-pressure semiconductor materials was also presented.
- **Chapter 4** presents the methodology and computational parameters used for this study.
- **Chapter 5** contains the results obtained in this study. The structural properties, stability of defects and electronic properties are presented.
- **Chapter 6** consists of the important conclusions from the obtained results. Recommendations for future work are also presented in this chapter.

CHAPTER 2

Electronic structure methods and calculations

In this section, a concise report of the theory behind the vital components of the electronic structure methods employed in this work are discussed.

2.1 Variational principle

The variational theory states that the expectation value of the energy operator is determined from any trial function Ψ_{trial} obeying the same boundary condition. This is due to the fact that the correct wave function of the system cannot be lower than the exact ground state energy E_{gs} of the system, with Hamiltonian $\hat{H}$ [16]. The variation principle is expressed as;

$$\frac{\int \Psi^*_{trial}(\vec{r})\hat{H}\Psi_{trial}(\vec{r})d^3\vec{r}}{\int \Psi^*_{trial}(\vec{r})\Psi_{trial}(\vec{r})d^3\vec{r}} \geq E_{gs}. \tag{2.1}$$

2.2 Many-body Hamiltonian

The properties of matter at the nanoscale are described by the laws of quantum mechanics. Quantum mechanics has been used to provide a description of matter beyond the classical including systems on the atomic scale. A system can be described by its wave-function, Ψ, which contains the probability amplitude for each configuration of the constituent particles [17]

$$\Psi(\vec{r}_1, \vec{r}_2, \ldots, \vec{r}_N, \vec{R}_1, \vec{R}_2, \ldots, \vec{R}_I), \tag{2.2}$$

where r_N are positions (including spin information) for all N electrons and R_I are positions for all I nuclei. The behaviour of atoms and electrons in a system evolving with time is governed according to the time-dependent Schrödinger equation [18].

$$i\hbar\frac{\partial}{\partial t}\Psi = \hat{H}\Psi \tag{2.3}$$

where i is the imaginary unit and $\hbar$ is the Planck's constant divided by 2π, $\hat{H}$ the Hamiltonian operator characterizes the total energy of any given wave-function and takes different forms depending on the situation. The symbol "$\frac{\partial}{\partial t}$" indicates a partial derivative with respect to time t. When considering a stationary situation, the Hamiltonian is independent of time, the time-independent Schrödinger equation simply takes the form:

$$E_i\Psi = \hat{H}\Psi_i \tag{2.4}$$

where the many-body wavefunction is represented by Ψ_i which corresponds to the i^{th} state with energy E_i. The Hamiltonian $(\hat{H})$ of interacting electrons and nuclei within a condensed matter system can be described as

$$\hat{H} = \frac{-\hbar^2}{2_{me}}\sum_i \bigtriangledown_i^2 - \frac{1}{2}\sum_I \frac{\hbar^2}{M_I}\bigtriangledown_I^2 - \sum_{i,I}\frac{Z_I e^2}{|\vec{r}_i - \vec{R}_I|} + \frac{1}{2}\sum_{i\neq j}\frac{e^2}{|\vec{r}_i - \vec{r}_j|} + \frac{1}{2}\sum_{I\neq J}\frac{Z_I Z_J e^2}{|\vec{R}_I - \vec{R}_J|} \tag{2.5}$$

Where the terms associated with the nuclei are denoted by upper case subscripts (I and J) and the electron terms are denoted by lower case subscripts (i and j). The masses and charge of the nuclei are represented as M_I and Z_I respectively while the mass of the electron is represented as m_e. The positions of the I^{th} nucleus and i^{th} electron are denoted by $\vec{R}_I$ and $\vec{r}_i$ respectively. The first two terms describe the kinetic energy of the electrons and nuclei. The other three terms represent the attractive electrostatic interaction between the electrons and the nuclei and the repulsive potential due to the electron-electron and nucleus-nucleus interactions.

Several meaningful approximations are necessary to make the many-body problem docile, as the solution to this problem within the exact quantum mechanical framework is practically impossible. Some of these meaningful approximations are described as follows.

2.3 Born-Oppenheimer approximation

Born and Oppenheimer [19] suggested a condition under which electronic and nucleic degrees of freedom in many atom (electron) system can be justifiably separated from each other. The Born-Oppenheimer approximation (BOA) assumed that since the nuclei are much more massive than the electrons, the motion of the electrons are rapid compared with the motion of the nuclei. Thus, the nuclei can be assumed to be clamped at fixed inter-nuclear distances R_{IJ}. Hence, the electrons are in motion in the field of the nuclei whereas the nuclei are in motion in the electronic potential surfaced as E_{total} [20].

The approximation allows the dynamics of the electrons and nuclei to be approximately decoupled as such we get independent wave-function for electrons Ψ_e and nuclei Ψ_n, with energies E_e and E_n respectively. Based on the approximation, the Hamiltonian of the many-body electronic problem, Equation (2.5) is then approximated to the electronic Hamiltonian of a fixed nuclei configuration R [19].

$$\hat{H}_{B-O}(R) = -\frac{1}{2}\sum_{i} \nabla_i^2 - \sum_{i,I} \frac{Z_I}{|\vec{r}_i - \vec{R}_I|} + \frac{1}{2}\sum_{i \neq j} \frac{1}{|\vec{r}_i - \vec{r}_j|} \tag{2.6}$$

where the first, second and third terms represents the kinetic energy of the electrons, the electron-nucleus Coulomb interaction and the electron-electron Coulomb interaction respectively. The expression $\frac{1}{2}\sum_{I \neq J} \frac{Z_I Z_J}{|\vec{R}_I - \vec{R}_J|}$, known as the nucleus-nucleus Coulomb interaction, is not included because it is a constant for a fixed ionic configuration R and thus, results in only a simple shift of the BOA energy eigenstates [21]. The time independent

Schrödinger equation for the electronic motions is now

$$\hat{H}_e \Psi_e(\vec{r}, \vec{R}) = E_e \Psi_e(\vec{r}, \vec{R}). \tag{2.7}$$

From the Equation (2.7), the term $\Psi_e(\vec{r}, \vec{R})$ describes the motion of the electrons and depends explicitly on the electronic coordinates ($\vec{r_i}$) and parametrically on the nuclei coordinates ($\vec{R_I}$) [22]. Note that the parametric dependence of Ψ_e on $\vec{R_I}$ was explicitly omitted from Equation (2.5) of the BOA. The total energy can then be written as;

$$E_{total} = E_e + E_n \tag{2.8}$$

Now, since the electronic wave-function Ψ_e, depends parametrically on only the nuclei coordinates ($\vec{R_I}$), it implies that for a fixed configuration of the nuclei, $\vec{R_I}$ is suppressed and the many-electron wave-function, $\Psi_e = \Psi_e(\vec{r}_1, \vec{r}_2, \ldots, \vec{r}_N)$ describing the system's electronic states is subjected to two conditions; they must be normalized

$$\langle \Psi_e | \Psi_e \rangle = \int \int \cdots \int |\Psi_e|^2 d\vec{r}_1 d\vec{r}_2 \ldots d\vec{r}_N = 1 \tag{2.9}$$

and antisymmetric with respect to interchange of any two electrons i and j

$$\Psi_e(\ldots, \vec{r}_i, \ldots, \vec{r}_j, \ldots,) = -\Psi_e(\ldots, \vec{r}_j, \ldots, \vec{r}_i, \ldots,) \tag{2.10}$$

The state Ψ_e of interest, is the ground state wave-function Ψ_0 with energy E_0. It is the lowest energy solution to the electronic part of the Schrödinger Equation (2.7). The many-body Equation (2.6) contains two-body Coulomb terms and the exchange correlation (in the third term) and thus, requires further simplification. One of the earliest approximations that helped in solving Equation (2.7) is the Hartree approximation [23].

2.4 Hartree approximation

Hartree proposed that a simple possible ansatz is to construct the many-body wave-function as a product of one-electron wave-functions $[\psi(\vec{r}_i)]$ [23].

$$\Psi_e(\vec{r}_1, \vec{r}_2, \cdots, \vec{r}_n) = \psi_1(\vec{r}_1), \psi_2(\vec{r}_2), \cdots, \psi_N(\vec{r}_N) \tag{2.11}$$

The Hartree approximation (HA) was derived in 1928. In the Hartree approximation, it is assumed that the eigenstates of the total Hamiltonian can be written as a product of single particle states. An equation for these single particles can then be derived using the variational approximation. The HA [23] started from the idea that the effect of the electron-electron interaction on a certain electron at position $\vec{r}$, should approximately be given by the electrostatic potential, which is generated by all other electrons on average at position $\vec{r}$. The approximation replace the potential $\hat{V}_{e-e}(\{\vec{r}\})$ of the many-body Schrödinger equation

$$\hat{V}_{e-e}(\{\vec{r}\}) \approx \sum_i \upsilon^{hartree}(\vec{r}_i), \tag{2.12}$$

with the

$$\upsilon^{hartree}(\vec{r}) = \sum_{i \neq j} \int \frac{n_i(\vec{r})}{|\vec{r}_i - \vec{r}_j'|} \, d.\vec{r} \tag{2.13}$$

Where $\upsilon^{hartree}(\vec{r})$ of Equation (2.13) is known as the Hartree potential. The ansatz of Equation (2.12) is known as the mean field approximation. As a result, the many-body Hamilton operator disintegrate into N single-particle operators

$$\hat{H}_e = \sum_{i=1}^{N} \hat{h}(\vec{r}_i) \tag{2.14}$$

where each electron would then be described by an effective single-particle Schrödinger equation with a Hamilton operator

$$\hat{h} = -\frac{\hbar^2}{2m} \bigtriangledown^2 + v(\vec{r}) + v^{hartree}(\vec{r}). \tag{2.15}$$

2.4.1 Hartree-Fock approximation

The ansatz given by Equation (2.11) leads to the Hartree product which is not in use any more because it neglects an important property of electrons – the fact that electrons are indistinguishable Fermions and the wave-function of a system of identical fermions must be antisymmetric with respect to interchange of any pair of particles according to Equation (2.10). This antisymmetric requirement is not satisfied by Equation (2.11).

The Hartree-Fock approximation follows directly from the Hatree approximation, taking into account the need for anti-symmetric states for Fermions. The Hamiltonian for the system is the same as for the Hartree approximation. The exchange requirement on the system of particles will add an extra interaction term in the final result. The Hartree-Fock method is more about solving complex many-body problems numerically from the study of effective non-interacting particle model as it gives important insight into the properties of many-electron systems [24].

The one-electron functions $\psi(\vec{r}_i)$ are called spin orbitals, and are composed of a spatial orbital $\phi_1(\vec{r}_i)$ and one of the two spin functions, $\alpha(s)$ or $\beta(s)$

$$\psi(\vec{r}) = \phi(\vec{r})\sigma(s), \qquad \sigma = \alpha, \beta \tag{2.16}$$

The spin orbitals are usually chosen to be orthonormal because the spin functions can be orthonormalised, i.e., $\langle\alpha|\alpha\rangle = \langle\beta|\beta\rangle = 1$ and $\langle\alpha|\beta\rangle = \langle\beta|\alpha\rangle = 0$. Hence, we have;

$$\langle\psi_i(\vec{r})|\psi_j(\vec{r})\rangle = \int \psi_i^*(\vec{r})\psi_j^*(\vec{r})\, d\vec{r} = \delta_{ij} \tag{2.17}$$

The limitation in Equation (2.11) can be rectified by forming a new wave function which is a linear combination of Hartree products in the form of a determinant called a Slater determinant, named after John Slater [25]. This forces the wave-function to obey Equation (2.10) as proposed by Fock [23]. For two particles, it is given as:

$$\Psi_e(\vec{r}_1, \vec{r}_2) = \frac{1}{\sqrt{2}}[\psi_1(\vec{r}_1)\psi_2(\vec{r}_2) - \psi_1(\vec{r}_2)\psi_2(\vec{r}_1)] = -\Psi_e(\vec{r}_2, \vec{r}_1) \tag{2.18}$$

The factor $\frac{1}{\sqrt{2}}$ is introduced to preserve the normalization. In this way, the Pauli exclusion principle is also satisfied. Considering a general case, if there are N electrons, then there are $N!$ possibilities to interchange that. This results in a fully antisymmetric wave-function:

$$\Psi_e(\vec{r}_1, \vec{r}_2, \cdots, \vec{r}_n) = \frac{1}{\sqrt{N!}} \sum_p (-1)^p \cdot \psi_{p_1}(\vec{r}_1)\psi_{p_2}(\vec{r}_2)\cdots\psi_{p_N}(\vec{r}_N) \tag{2.19}$$

P runs over all permutations of electrons, $(-1)^p = 1$ for even permutations and $(-1)^p = -1$ for odd permutations of the labels $1, 2, \ldots, N$. It is convenient to write down the wave-functions as determinants

$$\Psi_e(\vec{r}_1, \vec{r}_2, \cdots, \vec{r}_n) = \frac{1}{\sqrt{N!}} \begin{vmatrix} \psi_1(\vec{r}_1) & \psi_2(\vec{r}_1) & \cdots & \psi_N(\vec{r}_1) \\ \psi_1(\vec{r}_2) & \psi_2(\vec{r}_2) & \cdots & \psi_N(\vec{r}_2) \\ \vdots & \vdots & \ddots & \vdots \\ \psi_1(\vec{r}_N) & \psi_2(\vec{r}_N) & \cdots & \psi_N(\vec{r}_N) \end{vmatrix} \tag{2.20}$$

The wave-function of this form is called a Slater determinant. In the Slater determinant each of the columns are labelled by spin orbitals. Exchange of two electron coordinates will interchange two columns in the determinant. This satisfies the anti-symmetric requirement by introducing a negative sign. Using the Hartree-Fock wave-function, the

electronic energy can now be written as;

$$E_e^{HF} = \langle \Psi_e^{HF} | H^e | \Psi_e^{HF} \rangle = \sum_{i=1}^{N} h_i + \frac{1}{2} \sum_{i,j=1}^{N} h_i (J_{ij} - K_{ij}) \tag{2.21}$$

where

$$h_i = \int \psi_i^*(\vec{r})[-\frac{1}{2} \bigtriangledown^2 + V(\vec{r})]\psi_i(\vec{r})\, d(\vec{r}) \tag{2.22}$$

$$J_{ij} = \iint \psi_i^*(\vec{r})\psi_j^*(\vec{r\prime}) \frac{1}{|r - r'|} \psi_j(\vec{r})\psi_i(\vec{r\prime})\ \ d(\vec{r})(\vec{r\prime}) \tag{2.23}$$

$$K_{ij} = \iint \psi_i^*(\vec{r})\psi_j^*(\vec{r\prime}) \frac{1}{|r - r'|} \psi_j(\vec{r})\psi_i(\vec{r\prime})\ \ d(\vec{r})(\vec{r\prime}) \tag{2.24}$$

The integrals of Equations (2.22) to (2.24) are all real, and $J_{ij} \geq K_{ij} \geq 0$. J_{ij} are called Coulomb integrals while the K_{ij} are called exchange integrals. This leads to a mapping from a complex N-electron Schrödinger equation into an effective one-electron Schrödinger-like equations.

$$\hat{F}_i \psi_i(\vec{r}_i) = \epsilon_i \psi_i(\vec{r}_i), \hat{F}_i = -\frac{1}{2} \bigtriangledown^2 + V(\vec{r}_i) + V_H(\vec{r}_i) + V_{\vec{r}}(\vec{r}_i) \tag{2.25}$$

According to Equation (2.25), $\hat{F}_i$ is a one-electron Hamiltonian, known as the Fock operator while ϵ_i and ψ_i are the corresponding eigenvalues and eigenvectors, respectively. The first two terms ($-\frac{1}{2}\bigtriangledown^2$ and $V(\vec{r}_i)$) in $\hat{F}_i$ are, respectively, the kinetic energy of an electron and the external potential. The external potential, $V(\vec{r}_i)$, is the Coulomb attraction on the i^{th} electron due to the nuclei. The third and fourth terms approximately account for the many-body electron-electron interactions. The $V_H(\vec{r}_i)$ is the Hartree potential, which is the Coulomb repulsion between the i^{th} electron and the electron density produced by the remaining $(N-1)$ electrons.

$$V_H(\vec{r}_i) = \iint \frac{n(\vec{r}_j)}{|r_i - r_j|}\, d\vec{r}_j, \quad n(\vec{r}_j) = \sum_{j=1}^{N} |\psi_j(\vec{r}_j)|^2 \tag{2.26}$$

$n(\vec{r}_j)$ in Equation (2.26), represents the probability density of the j^{th} particle. The fourth term of Equation (2.25) solely appears from the anti-symmetric nature of the wave-function and is known as exchange potential $V_{\vec{r}}(\vec{r}_i)$. $V_{\vec{r}}(\vec{r}_i)$ does not have any classical analogy, and can only be written as an integral operator, unlike $V(\vec{r}_i)$ and $V_H(\vec{r}_i)$.

$$V_{\vec{r}}(\vec{r}_i)\psi_i(\vec{r}_i) = \left[\sum_{j=1}^{N} \int \psi_j^*(\vec{r}_j) \frac{1}{|r_i - r_j|} \psi_i(\vec{r}_i)\, d(\vec{r}_j)\right] \psi_j(\vec{r}_j) \tag{2.27}$$

Equation (2.25) is the usual form of the Hartree-Fock equation, which is a linear eigenvalue problem that must be solved self consistently. The Hartree-Fock method is extensively used to study various materials science problems, such as adsorption [26], defects in solids [27], and electronic structure of insulators [28].

A major drawback of the Hartree-Fock approximation lies in the effective mean-field treatment of the Coulomb repulsion between electrons, which provides an inaccurate description of the spatial separation of the electrons as it would be in a complete many-electron interaction. This missing part is extensively termed "correlation" [29]. The Hartree-Fock approximation gave an erroneous prediction that the electronic density of states vanishes at the Fermi level. The incorrect prediction made was as a result of neglecting the Coulomb repulsion felt by all electrons of opposite spin. Numerous approaches which explicitly calculate the electron correlation were employed to resolve this shortcoming. One of these approaches known as density functional theory, which takes into consideration the effects of both exchange and correlation energy will be described in the following section.

2.5 Density functional theory

Density functional theory (DFT) is a modern approach to the solution of many-body quantum mechanical problems in solid state. It is built upon two theorems proposed by Hohenberg and Kohn in 1964. The DFT considers some important terms not considered in earlier

computational methods, such as the Hartree-Fock method. DFT, based on Hohenberg-Kohn (HK) theorems [30] and Kohn-Sham (KS) equations [31], is presently the most widely used method to compute the total energy and electronic structure of matter. The DFT uses basic variable including the ground state electron density $n_o(\vec{r})$ of the system, rather than the many electrons wave-functions. DFT further suggests that the electronic density of a system is key to obtaining useful information on its various properties. The huge computational cost associated with the large number of slater determinants for a many-body system is thus saved in this approach. The two Hohenberg-Kohn theorems described next, show that the spatially dependent electron density $n(\vec{r})$ is sufficient to determine the ground state energy and properties of the system.

2.5.1 Hohenberg-Kohn formalism

The many-electron wave-function is too complicated to deal with, because it is a function of $3N$ variables. In 1964, Hohenberg and Kohn proposed and proved two important theorems that enable the electron density to be used in order to provide an exact theory for many-body systems.

Theorem 1: *For any system of interacting particles in an external potential $v_{ext}(\vec{r})$, the potential $v_{ext}(\vec{r})$, is determined uniquely, except for a constant, by the ground state particle density $n_o(\vec{r})$.* [32]

Theorem 2: *A universal functional for the energy $E[n(\vec{r})]$ in terms of the density $n(\vec{r})$ can be defined for any external potential $v_{ext}(\vec{r})$, and for any particular $v_{ext}(\vec{r})$, the ground state energy of the system is the global minimum value of this functional, and the density $n(\vec{r})$ that minimizes the functional is the exact ground state density $n_o(\vec{r})$* [32].

Considering an electronic system with a given Hamiltonian where the ground state electron density determines the number of electrons, it follows that the density determines

the wave-function and thereby all the ground state properties of the system. The total ground state energy, the ground state kinetic energy, the energy of the electrons in the external potential $v_{ext}(\vec{r})$ and the electron-electron interaction energies are all functions of the density $n(\vec{r})$. Thus the total energy functional $E[n(\vec{r})]$ in the second Hohenberg and Kohn theorem can be written in terms of the given external potential $v_{ext}(\vec{r})$ as follows;

$$E[n(\vec{r})] = \int v_{ext}(\vec{r})n(\vec{r})d\vec{r} + F[n(\vec{r})]. \tag{2.28}$$

Where $F[n(\vec{r})]$ is explicitly independent of the system, and is called the Hohenberg-Kohn functional for the kinetic energy $T[n(\vec{r})]$, of the electrons and the electron-electron interaction (v_{e-e}). Thus $F[n(\vec{r})]$ can be written as;

$$F[n(\vec{r})] = \langle \Psi | n | T + v_{e-e} | \Psi | n \rangle. \tag{2.29}$$

Hohenberg-Kohn theorems reduce the problem of finding the physical properties associated with the ground state of a system to obtaining the electron density that minimises the energy functional [33]. However, the two theorems do not offer a way of computing the $F[n(\vec{r})]$, and thus no practical way of determining the ground state energy of the system. This limitation was however subdued by the mathematical expression developed by Kohn and Sham [31].

2.5.2 The Kohn-Sham equations

Kohn et al., proposed a method (similar to the Hartree-Fock approach) for computing the kinetic energy functional [33]. Kohn-Sham introduced a set of orbitals "Kohn-Sham orbitals" through which the electron density and kinetic energy can be evaluated. The Kohn-Sham orbitals in general, do not correspond to the actual electron orbitals and its eigenvalues are not the same as the real energy levels. The only connection the Kohn-Sham orbitals have to the real electronic wavefunctions is that, they both give rise to

the same charge density. Their idea was to map the tricky system of many interacting electrons on to an auxiliary system of non-interacting Kohn-Sham particles moving in an effective potential. This reduced the many-electron Schrödinger equation to equations for one-electron wave functions called Kohn-Shams equation.

Kohn and Sham proposed a new reformulation of the energy functional, Equation (2.28), in order to find an analytical solution for it [31]. The functional $F[n(\vec{r})]$ was separated into three distinct parts:

$$F[n(\vec{r})] = T[n(\vec{r})] + E_H[n(\vec{r})] + E_{xc}[n(\vec{r})]. \tag{2.30}$$

Where the first term, $T[n(\vec{r})]$, is the kinetic energy functional for a system of non-interacting electrons producing the same density as $n(\vec{r})$. The $T[n(\vec{r})]$ is defined as

$$T[n(\vec{r})] = -\frac{1}{2}\sum_{i=1}^{N}\int \psi_i^*(\vec{r}) \bigtriangledown^2 \psi_i(\vec{r}) d\vec{r} \tag{2.31}$$

The second term, $E_H[n(\vec{r})]$, is the Hartree energy, arising classically from the mutual Coulomb repulsion of all electrons and is expressed as:

$$E_H[n(\vec{r})] = \frac{1}{2}\iint \frac{n(\vec{r})n(\vec{r}')}{|\vec{r}-\vec{r}'|} d\vec{r}d\vec{r}' \tag{2.32}$$

The last term, $E_{xc}[n(\vec{r})]$ of Equation (2.30), is a correction term called the exchange-correlation functional, which accounts for all the many-body effects in $F[n(\vec{r})]$. The functional form of the correction term $E_{xc}[n(\vec{r})]$ is unknown and must be approximated. Practical applications of DFT are therefore classified according to the approximations taken for the exchange-correlation functional $E_{xc}[n(\vec{r})]$.

The final Kohn-Sham solution is attained using an iterative method, whereby the Schrödinger equation is solved for individual electrons and paving the way for a new effective potential to be obtained. The obtained effective potential is then used to compute the electron density which consequently generates a new effective potential. This

process of solving the Schrödinger equation continually and generating a new effective potential is continued until the minimum energy of the system changes by less than a set limit. The iterative procedure used for this process is the **Self Consistent Field (SCF)** approach as shown in Figure 2.1.

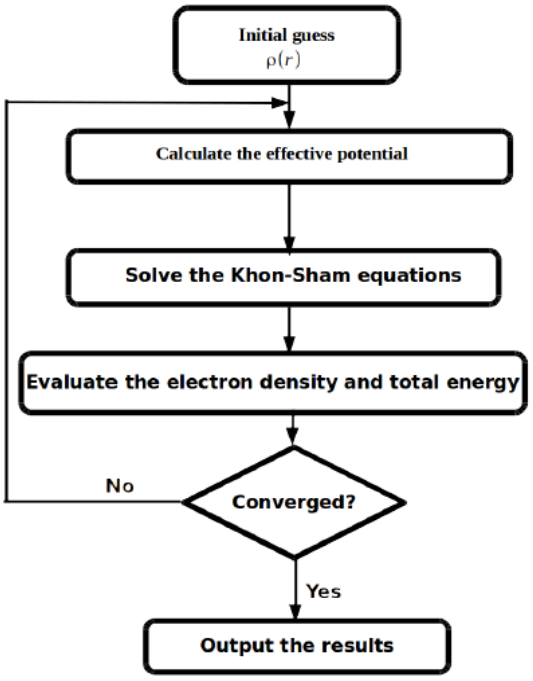

Figure 2.1: A schematic flow chart illustrating the self consistent field calculation of the DFT [47].

2.6 Exchange-correlation functionals

The exchange-correlation (E_{xc}) is the energy contribution from the quantum effects that is not included in the Coulomb repulsion and the single-particle kinetic energy. For practical use of the Kohn-Sham equations, we must know what the form of the exchange-correlation energy functional is. However, the exact exchange-correlation energy is unknown and hence it needs to be approximated. Commonly used approximations include the local density approximation (LDA) [31], generalized gradient approximation (GGA) [34], hybrid functionals. Other notable exchange-correlation functionals are the LDA+U [35] and GGA+U [36]. These approximations are discussed in the following sub-sections;

2.6.1 The local density approximation

The local density approximation (LDA) uses only the electron density, $n(\vec{r})$, at a spatial point $\vec{r}$ to determine the exchange-correlation energy at a point. The exchange-correlation energy density is taken to be that of the uniform electron gas of the same density. In the LDA regime, the exchange correlation functional is approximated as

$$E_{xc}^{LDA}[n] = \int n(\vec{r})\varepsilon_{xc}^{hom} n(\vec{r}) d(\vec{r}) \tag{2.33}$$

where ε_{xc}^{hom} is the exchange-correlation energy per particle of the interacting uniform electron gas with the density $n(\vec{r})$. The uniform electron gas represents a family of systems of interacting electrons with an arbitrary spatially constant density $n(\vec{r})$ that acts as a parameter.

For a homogeneous electron gas, the exchange energy is given by;

$$\varepsilon_{xc}^{hom} = \frac{-e^2}{4\pi\varepsilon}\frac{3}{4}\left(\frac{3n}{\pi}\right)^{\frac{1}{3}} \tag{2.34}$$

One of the major deficiency of the LDA is its inability to predict accurately the band gap of solid materials.

2.6.2 The generalized gradient approximation

It was realized that only the local uniform density at each given point is not a reasonable approximation for the rapidly varying electron densities of many materials, and that the gradient of the density $(\bigtriangledown(\vec{r}))$ needs to be included. The generalized gradient approximation (GGA) goes beyond LDA by using not just the information about the density at a particular point $n(\vec{r})$, but also adding the gradient of the density, $|(\bigtriangledown(\vec{r}))|$, as an independent variable. Within this approximation, the non-homogeneity of the true electron density is considered and the exchange-correlation functional $(E_{xc}^{GGA}[n])$ at a particular

point is written as

$$E_{xc}^{GGA}[n] = \int n(\vec{r})\varepsilon_{xc}(n(\vec{r}), \bigtriangledown n(\vec{r}))d(\vec{r}) \tag{2.35}$$

The gradient introduces non-locality into the description of the exchange and correlation. This can improve the functional's performance greatly by helping to account for fast varying changes in the electron density that are not well described by the local density approximation. One of the major deficiency of the GGA is its inability to predict accurately the band gap of solid materials. For example, the GGA has been use to wrongly predict Ge as a metal.

2.6.3 Hybrid functionals

The LDA and GGA underestimate band gaps especially for small gap systems, thereby making structural properties related to the band gap difficult to predict. Their failure in predicting accurately the band gap of several materials and other properties in semiconductor materials [37] has been corrected by hybrid functionals. Hybrid functionals which incorporate a portion of the exact exchange from Hartree-Fock theory with the exchange and correlation from other sources (empirical or ab initio) was introduced by Becke in 1993 [38]. The hybrid exchange-correlation energy functional $E_{xc}^{hyb}[n]$ is defined as

$$E_{xc}^{hyb}[n] = \alpha E_x^{HF}(\omega) + E_c^{GGA} - (\alpha - 1)E_x^{GGA} \tag{2.36}$$

where E_x^{HF} is the exact non-local Hartree-Fock exchange energy, E_c^{GGA} and E_x^{GGA} are the semilocal GGA correlation and exchange functionals respectively, α is a mixing parameter and ω is an adjustable parameter. One of the most commonly used versions of hybrid functional among quantum chemists is B3LYP, which stands for Becke, 3-parameter, Lee-Yang-Parr [39].

$$E_{xc}^{B3LYP} = E_{xc}^{LDA} + a_0(E_x^{HF} - E_x^{LDA}) + a_x(E_x^{GGA} - E_x^{LDA}) + a_c(E_c^{GGA} - E_c^{LDA}) \tag{2.37}$$

Where $a_0 = 0.20$, $a_x = 0.72$, and $a_c = 0.81$. E_{xc}^{LDA}, E_x^{HF} and E_x^{LDA} are the LDA exchange-correlation energy functional, Hartree-Fock exchange energy functional and LDA exchange functional respectively, and E_x^{GGA} and E_c^{GGA} are respectively the GGA exchange and correlation functionals.

Another popular version is the PBE0 functional [34] which includes 25% of Hartree-Fock exchange and is defined as:

$$E_{xc}^{PBE0} = 0.25E_x^{HF} + 0.75E_x^{PBE} + \Delta E_c^{PBE} \tag{2.38}$$

where E_x^{PBE} and E_c^{PBE} respectively denote the exchange and correlation parts of the PBE density functional.

2.7 Pseudopotential

The many-electron Schrödinger equation can be simplified if electrons are divided into two groups: valence electrons and inner core electrons. The electrons in the inner shells are strongly bound and do not play a significant role in the chemical binding of atoms. The pseudopotential approach is a method employed to construct an effective potential that will replace the atomic all-electron potential such that, the cores states are eliminated and the valence electrons are described by pseudo-wavefunctions. This comes from the fact that the core electrons are frozen, and can be considered together with the nucleus as a single effective nucleus. This makes it possible to treat Equation (2.25) within the context of nearly-free electron model, where the wavefunctions are the plane-wave basis set.

The use of pseudopotentials was first introduced by Fermi in 1934. The main drawback of using a pseudopotential in contrast to an all-electron method is that it compromises the universality of the method. A pseudopotential must do its best to accurately reflect the interaction between core and valence electrons, in all the different possible environments into which an atom could be placed. This is known as the transferability of the pseu-

dopotential. There are different kinds of pseudopotentials which are discussed in the next section.

2.7.1 Norm-conserving pseudopotentials

Norm-conserving pseudopotentials [40] ensure that the charge within the cut-off region is equal to the charge of the core electrons. In essence, the core region of the atom is not greatly affected by the surrounding environment and so aids transferability. The potential is constructed in such a way that within the cut-off radius, it satisfies the normalization condition of the atomic all-electron wavefunctions $(\psi_{a,i})$. The norm-conserving condition is given by:

$$0 = \langle \psi_{p,i} | \psi_{p,j} \rangle - \langle \psi_{a,i} | \psi_{a,j} \rangle \tag{2.39}$$

2.7.2 Ultra-soft pseudopotentials

Ultra-soft pseudopotentials [41], results in more even Kohn-Sham wave-functions and thus require less plane-waves. In ultra-soft pseudopotentials method, the cut-off radius is larger, compared to that of the norm-conserving pseudopotentials. The potential is constructed in such a way that the norm-conserving constraint is relaxed [42] and the condition can generally be written as

$$0 \neq \langle \psi_{p,i} | \psi_{p,j} \rangle - \langle \psi_{a,i} | \psi_{a,j} \rangle \tag{2.40}$$

Pseudopotentials calculations have some limitations for all systems where the overlap between valence- and core- electron densities is not completely negligible. This is due to the non-linearity of the exchange interaction between the valence and core electrons. This shortcoming may be removed by using the projector-augmented wave method.

2.7.3 The projector-augmented wave method

The projector-augmented wave (PAW) method [43] uses plane-waves in between atoms and a localized basis close to the atoms. The PAW can be a more transferable method than a pure plane-wave implementation because it has access to the full all-electron wave-function. The PAW can produce more accurate results than a frozen core approximation. However, engaging the plane-waves for most of the system helps keep the computational cost down and retains the attractiveness of a single convergence parameter, called the Plane-wave cut-off.

2.8 Basis set

In order to solve the single-particle Kohn-Sham equations, the single-electron wave-functions must be expanded in terms of a basis. This helps to transform the differential single-particle Schrödinger equations into a matrix equation. There are two broad classes of modern electronic structure which depend on the choice of the basis set used for the expansion of the valence orbitals and charge densities. These are localized atomic orbitals and plane-waves basis sets. Plane-waves basis sets are usually considered for studies that involve matter in condensed phases. This is because the plane-wave basis is complete and simplify the computation of force and stress tensor of a system [44]. They enable the use of fast Fourier transforms to move between real space and k-space. Furthermore, operations become much faster and also, the Hellmann-Feynman theorem can be used to calculate the forces directly as the Plane-Waves do not depend on the position of the atoms [45, 46].

2.9 Brillouin zone

The Brillouin zone (BZ) is the Wigner-Seitz cell of the reciprocal lattice. It is defined by the planes that are perpendicular bisectors of the vectors from the origin to the recipro-

cal lattice points. The Bragg condition is satisfied on these planes for elastic scattering. However, incident particles with wavevectors inside the BZ has no Bragg scattering [32].

The Kohn-Sham orbitals are evaluated at a point k within the BZ, under periodic boundary conditions. A k-point is described as a reciprocal lattice vector, and it is used to label an electronic level (eigenstate). The K-point represents a position in the first BZ of a solid system. It is useful, under periodic boundary conditions, to convert the integral over the BZ into a summation over a set of discrete points of k-space [47]. The integral function $F(r)$ over the BZ is expressed as [48];

$$F(r) = \frac{V_{cell}}{(2\pi)^3} \int_{BZ} f(k) d\vec{k} = \sum_i \omega_i f(k) d\vec{k} \tag{2.41}$$

where V_{cell} is the unit cell volume, $f(k)$ is the Fourier transformation of $F(r)$ and ω_i is the weighting factor. For defects in semiconducting modelling, a large supercell is usually needed in semiconductors in order to avoid defect-defect interaction [47]. The volume of the Brillouin zone (V_{BZ}) of a crystal is related to the volume of the supercell (V_{Scell}) by

$$V_{BZ} = \frac{(2\pi)^3}{V_{Scell}} \tag{2.42}$$

From the Equation (2.42), the relationship shows that for a large supercell, the BZ volume is small, and consequently, less k-points are needed to sample it. An important concept used in BZ is the Monkhorst-Pack (MP) k-points spacing. The MP k-mesh is a set of k-points generated in an evenly spaced (k_x, k_y, k_z) grid spread through the BZ. The choice of the MP k-mesh is usually dependent on the crystal lattice, the space group symmetry and the supercell size.

CHAPTER 3

Literature review

This chapter provides a short review of defects in semiconductor. Furthermore, comprehensive review of first-principles studies of doping and defects in binary high-pressure semiconductor materials is presented.

3.1 Defects in material

There are no defect-free crystalline solids [49]. All crystalline solids contain various form of defects. Defects arise when there is a deviation from an orderly arrangement during solidification which may occur due to alloying elements, plastic deformation, grain boundaries [50]. These defects can be classified according to their geometries or dimensions as surface defect, linear defect and point defect. These different classes of defects are discussed in the following subsections.

3.1.1 Surface defects

Surface defects are irregular arrangement of atoms at grain boundaries. Atoms are arranged in a particular order in a grain. However, the directions of the arrangement are different in neighbouring grains. The boundaries are irregularly shaped (see Figure 3.1). Atoms are too far apart while at other places, they are too close than the normal distance, thus giving rise to tensile and compressive forces [51].

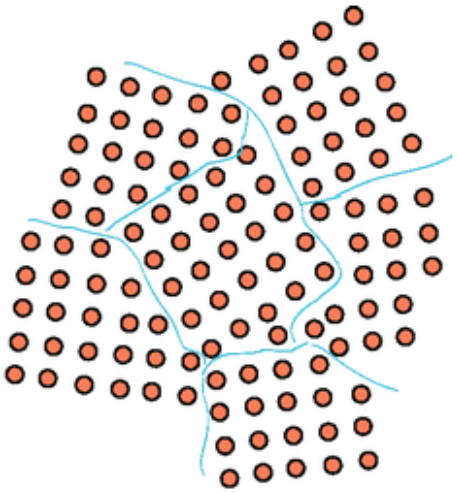

Figure 3.1: Grain boundaries [51].

3.1.2 Line defects (dislocations)

Dislocations are another type of defect in crystals. They are abrupt changes in the regular ordering of atoms, along a line called "dislocation line" in a solid. Dislocations are generated and move when a stress is applied [49]. The motion of dislocations allows slip – plastic deformation to occur [49]. There are two basic types of dislocations; the edge dislocation and the screw dislocation. Edge dislocations occur when an extra plane is inserted into a plane in the crystal lattice. Screw dislocations on the other hand, results when displacing planes are relative to each other through shear [49]. Actually, edge and screw dislocations are just extreme forms of the possible dislocation structures that can occur. Most dislocations are probably a hybrid of the edge and screw forms as shown in Figure 3.2.

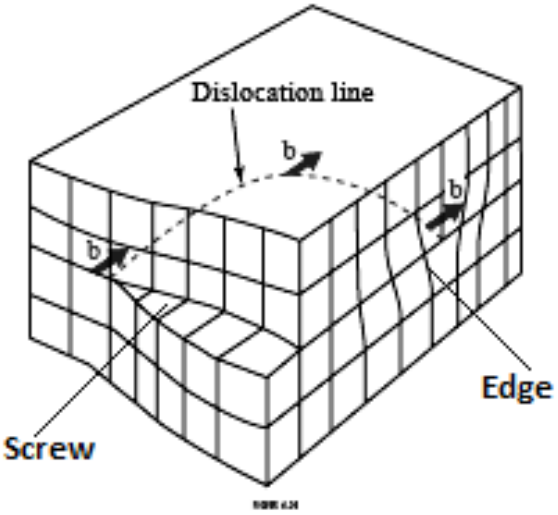

Figure 3.2: Mixed dislocation [49].

3.1.3 Point defect

Point defects in a crystalline solid may arise as a result of; (i) absence of an atom from a lattice point, (ii) an atom of a different element substituting an atom of parent metal, (iii) an atom getting to a site which is not a lattice point. Points defects include self-interstitial, substitutional and vacancies [49].

3.1.3.1 Interstitial

These atoms are much smaller than the atoms in the bulk matrix. An example of interstitial impurity atoms is the carbon atoms that are added to iron to make steel. A self-interstitial is an atom from the parent material that has crowded into an interstitial void in the crystal structure, as shown in Figure 3.3. Self-interstitial atoms distort and highly stress the tightly packed lattice structure. Hence, they occur only in low concentrations in metals. Self-interstitial as well as di-interstitial have been observed for several trilateral including Ge [52], Si [52] and other trilateral.

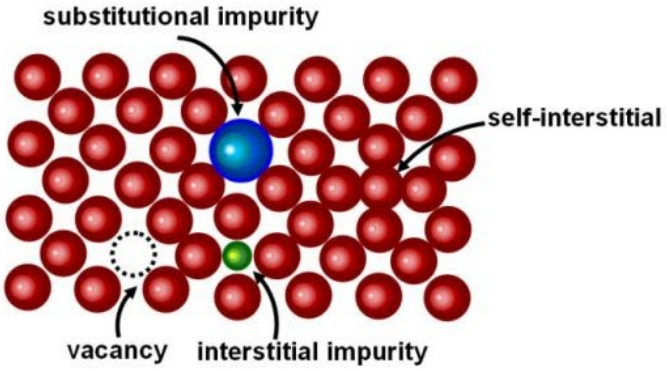

Figure 3.3: Point defects in crystalline lattices [51].

3.1.3.2 Substitutional defect

A substitutional atom is an impurity atom which replace or substitute for the host atoms as shown in Figure 3.3. Substitutional impurity atoms are usually close in size to the host atom. An example of substitutional impurity atoms is the zinc atoms in brass.

3.1.3.3 Vacancy

A vacancy exists in a crystal when there is an empty space. this could be caused by electron irradiation of material thereby hitting off atoms from their original position creating vacancy. Vacancy have been observe in several materials including Ge [53], Si [54], GaN [55]. Vacancies are common, especially at high temperatures when atoms are frequently and randomly changing their positions, leaving empty lattice sites behind.

3.2 Defects in AlSb and other alloys

Density functional study has been performed to understand effects of resistivity and carrier trapping on AlSb [13]. The effects of resistivity are important for radiation detection applications. Sb antisite (Sb_{Al}) is an important intrinsic defect in AlSb, which not only has low formation energy but also induces deep donor levels in the band of the host. This led to playing important role in carrier compensation. Furthermore, N impurity in AlSb

can pin the Fermi level without causing efficient carrier trapping whereas, O impurity in AlSb gives rise to a deep carrier-trapping level that may pin the Fermi level.

Wang et al., studied the electronic band structure of 6.1 Å family binary antimonide compounds and their ternary alloys [56]. Direct and indirect optical bowing properties and the crossover points in the AlGaSb and AlInSb ternary alloys were analysed. Band offsets between InAs and antimonide compounds was obtained in order to determine the transport and quantum confinement in the interface of a heterostructure. A band alignment of 1.56 eV between the conduction band minimum of the InAs and AlSb was obtained.

As reported by Andriotis and Menon, a predictive approach for band gap engineering involving substitutional doping of wide band gap semiconductors using an extension of Harrison's theory was developed and the approach was validated with $AlSb_{1-x}P_x$, $AlP_{1-x}Sb_x$, $GaN_{1-x}Sb_x$, $GaP_{1-x}Sb_x$, and $InP_{1-x}Sb_x$ systems [57]. The predictive results were then checked against ab initio ones obtained at the level of DFT/SGGA+U approximation and some of the predictive results were found to be in excellent agreement with corresponding ab initio ones. The minor discrepancies observed between the predicted and ab initio results were attributed to electronic processes not incorporated in Harrison's theory. Chroneos et al., reported reports based on the formation of antisite defects in III-V semiconductors (III = Al, Ga, and In and V = P, As, and Sb) [14]. The formation energies of group III antisites decrease with increasing covalent radius of only the group V atom, whereas the formation energies of group V antisites showed a consistent decrease with increase in both group III and group V covalent radii. The authors show that AlSb exhibits defect energies that are generally smaller than those in AlP or AlAs. Under Al-rich conditions, Al_{Sb} defects were more favourable compared to Sb_{Al}, allowing the Al antisites a wider range of stability with its lowest formation energy being 0.45 eV.

In 2016, Flores et al., reported the role of oxygen doping in CdTe as well as the formation energies, charge transition levels and quasiparticle defect states [58]. The researchers show that the incorporation of oxygen in CdTe leads to the formation of a new defect ($O_{Te} - Te_{Cd}$ complex) which is energetically favoured over both isovalent (O_{Te})

and interstitial oxygen (O_i) in the Te-rich limit. Furthermore, It was also observed that the presence of oxygen passivated the harmful deep energy levels associated with (Te_{Cd}), suggesting an improvement in the efficiency of CdTe based solar cells.

Diwaker and Kumar in a recent report doped pure zinc telluride (ZnTe) with antimony (Sb) atom to gain insight into the electronic properties and bandgap structures of ZnSbTe ternary compounds [59]. The authors show that the incorporation of Sb in ZnTe system introduces some bands which are primarily responsible for n-type and p-type conductivity. They further show that there is no gap state anywhere which indicates that ZnTe retains its semiconducting nature even after doping with Sb.

The energetic stability and electronic properties of substitutional C, Si and Ge impurities in [0001] GaN, AlN, and InN nanowires has been analysed via spin-polarized density functional theory [60]. The results show that carbon impurities in the cation site (i.e., $C_{Ga}, C_{Al}, and\ C_{In}$) exhibit lower formation energies at the surface of the nanowires leading to donor-like properties in GaN and InN nanowires. For the AlN nanowire, deep levels were observed inside the bandgap. In contrast, the carbon impurity C_N gave rise to a deep electronic level inside the nanowire bandgap. It was also observed that Si in GaN and InN; and Ge in InN are most stable at the cation site, leading to an n-type semiconductor property in the systems.

The influence of gallium impurities and their complexes on the electrical properties of ZnO has been studied [61]. The results showed that in O-rich environment, the formation energies complexes are significantly lower than that of the donor Ga_{Zn}. This suggest that experimentally observed high compensation ratios and lower conductivity, whereas in the O-poor environment, the complexes do not form, leading to a much larger value of carrier concentrations and conductivity. The resulting band gap due to the defects was reported to be 3.43 eV.

Nitrogen (N) doped zinc sulphide (ZnS) has been investigated using first principle calculations [62]. The results showed that nitrogen substituting sulphur (N_S) would induce paramagnetism in ZnS and an increase in band gap will cause the N_S defect to

induce ZnS to be a ferromagnetic metal. It was also noted that sulphur vacancies would give rise to ZnS with N_S defects system losing the magnetism. The total magnetic moment for ZnS supercell with single N_S defect was found to be 0.85 μB while the moderate formation energy of 0.71 eV obtained indicated that the ZnS with N_S defects could be fabricated experimentally.

In 2019, Chen et al., investigated the effect of Ti and Fe substitution doping on the magnetic properties of monolayer $CrSi_2$ by first-principle methods based on spin-polarized density functional theory [63]. The results reveal that: Ti-doped monolayer $CrSi_2$ is less stable than Fe-doped monolayer $CrSi_2$, the local magnetic moment of Ti and Fe atom all decreases compared with atomic moment in free gas phase and that the local magnetic moment of Fe atom is larger than Ti atom, causing the total magnetic moment of Fe-doped monolayer $CrSi_2$ to be bigger than that of Ti-doped monolayer $CrSi_2$. The authors deduced that both Fe- and Ti-doped $CrSi_2$ are magnetic and metallic.

The electronic structure of V doped $CrSi_2$ reveals that the valence band and conduction band close to the Fermi energy for pure $CrSi_2$ is comprised of 3d state electron of Cr and 3p state electron of Si [64]. However, for V-doped $CrSi_2$, the valence band and conduction band near the Fermi energy is mainly composed of 3d state electron of Cr and impurity atom V. The results show that after doping $CrSi_2$ with V atom, the conductive type changed into a p type and the band gap decreased from 0.35eV (pure $CrSi_2$) to 0.25eV (V-doped $CrSi_2$).

CHAPTER 4

Methodology

This chapter presents the computational details as well as the methodology of this thesis. The test for supercell size, test of k-points and energy cut-off were as well presented.

4.1 Computational details

DFT electronic structure calculations as implemented in the Quantum Espresso package [65] was used for the modelling of electronic and structural properties of defects in AlSb. All calculations were carried out using the generalized gradient approximation (GGA) functional of Perdew, Burke and Ernzerhof (PBE) [34]. The ultrasoft pseudopotentials was used to separate the core from valence electrons. The supercell approach was adopted and used since it provides good description of the electronic structure of the host and defect systems. In order to accurately compute the properties of the AlSb system, tests of convergence for the supercell size, number of k-points and plane wave kinetic energy cut-off was carried out to determine the well converged k-point, cut-off energy $(\mathrm{E_{cut}})$ and supercell. The pristine 64 atom supercell was constructed from an optimised unit cell containing 4 atoms, with a 3×3×1 Monkhorst-Pack [66] k-point and 60 Ry plane wave cut-off of the wave function expansion.

4.2 Test of supercell size

A fully optimised unit cell of AlSb was used to construct the supercell used for the defect calculations. The size of the supercells are $2 \times 2 \times 1$, $3 \times 3 \times 1$, $4 \times 4 \times 1$ and $5 \times$

5×1 containing 16, 36, 64 and 100 atoms, respectively. Single vacancy was created in the aforementioned supercells and the formation energy results obtained. The formation energy E_{form} of the defect in each of the supercells was calculated with a k-point of $3\times3\times1$ and a 60 Ry kinetic energy cut-off. Thereafter, the E_{form} was plotted as a function of the supercell size as shown in Figure 4.1.

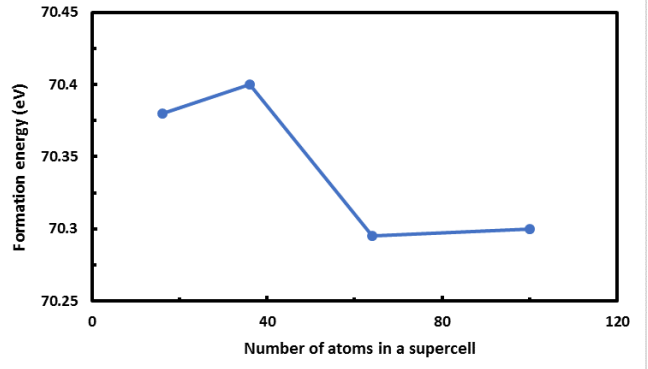

Figure 4.1: Plot of formation energy as a function of supercell for Al vacancy of AlSb. Here, the chemical potential was not taken into consideration since all the supercell required the same chemical potential.

4.3 Test of cut-off energy

To ascertain the most suitable energy cut-off (E_{cut}) for the plane wave, the total minimum energy with respect to different energy cut-off of 20, 40, 60, 80, 100, 120 and 140 Ry, was calculated using Monkhorst-Pack k-points of $3 \times 3 \times 1$ (see Figure 4.2). The difference in total energy converges adequately to within a 10^{-4} eV at energy cut-off of 60 Ry E_{cut}. The well converged energy cut-off of 60 Ry has been adopted for the results presented in this Thesis.

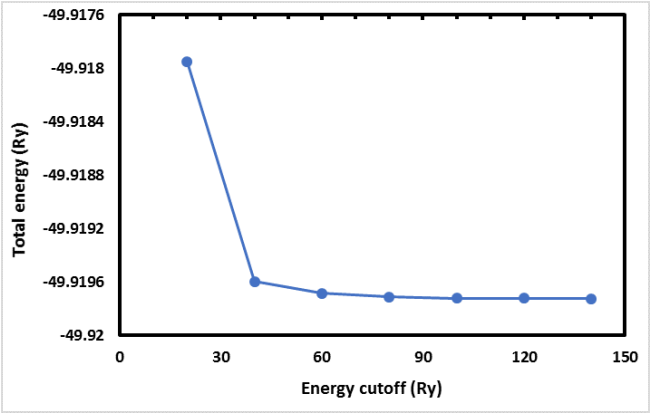

Figure 4.2: Plot showing the total energy as a function of the E_{cut} as a test of convergence.

4.4 Test of k-points

In order to sample the Brillioun zone, it is required to carried out a test for K-points. In this research, the test of k-points sampling was conducted for $(n \times n \times 1)$ positioned at gamma point, i.e to (0 0 0) for n = 2, 4, 6, 8, 10, 12, 14. The variation of the total minimum energy as a function of k-points was determined using an E_{cut} of 45 Ry. Figure 4.3 displays the results of the test of K-points.

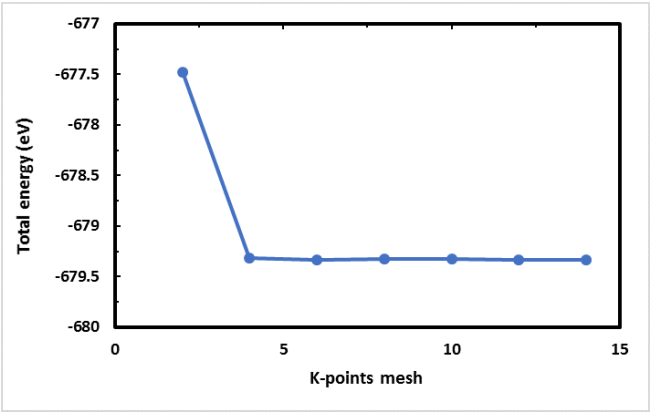

Figure 4.3: Convergence of total minimum energy of AlSb as a function of k-points sampling. (Kinetic energy cut-off of 45 Ry was used for the calculation).

Based on Figure 4.3, a well converged k-points spacing of $3 \times 3 \times 1$ was sufficient for the modelling of defects properties in this report.

4.5 Calculation details

According to Figure 4.1, using a $3 \times 3 \times 1$ Monkhorst-Pack k-point mesh is sufficient enough to carry out defect calculations because the formation energy difference between a $3 \times 3 \times 1$ and $4 \times 4 \times 1$ k-point mesh is less than 0.02 eV. Consequently, the Brillouin zone is sampled with $3 \times 3 \times 1$ Monkhorst-Pack grid for all systems. The Kohn-Sham equations were solved with plane wave basis sets and the energy band gap which is the difference between the Kohn-Sham eigenvalues for the lowest unoccupied and highest occupied orbitals are recorded and compared to experimental results where available. The stability of the defect in AlSb was predicted by calculating the defect formation energy as

$$E_{form} = E_{defect} - E_{pure} + \sum_{i} \Delta(n)_i \mu_i \tag{4.1}$$

where E_{defect} and E_{pure} are the total energies of the supercell with and without defect respectively. The $\Delta(n)_i$ is the difference in the number of atoms added or removed ($\Delta(n) < 0$, when an atom is added and $\Delta(n) > 0$, when an atom is removed) and μ_i is the chemical potential of the participating atom. The chemical potential is calculated as total energy per number of atoms in a system.

CHAPTER 5

Results

This chapter presents the result of this thesis. The results are categorized into the structural properties, stability and the electronic properties of defects in AlSb.

5.1 Structural properties

Five different defects in hexagonal 2D AlSb were investigated. The Sb vacancy (V_{Sb}), Al vacancy (V_{Al}) which are the intrinsic defects considered. Li and Be doped AlSb, where Li is substituted for Sb (Li_{Sb}) as well as Al atom (Li_{Al}), Be substitutes Sb (Be_{Sb}) and Be substitutes Al atom (Be_{Al}), were investigated.

Figure 5.1 displays the fully relaxed geometric structures of the pristine, vacancy and doped AlSb material. The AlSb alloy has a honeycomb structure as shown in Figure 5.1.

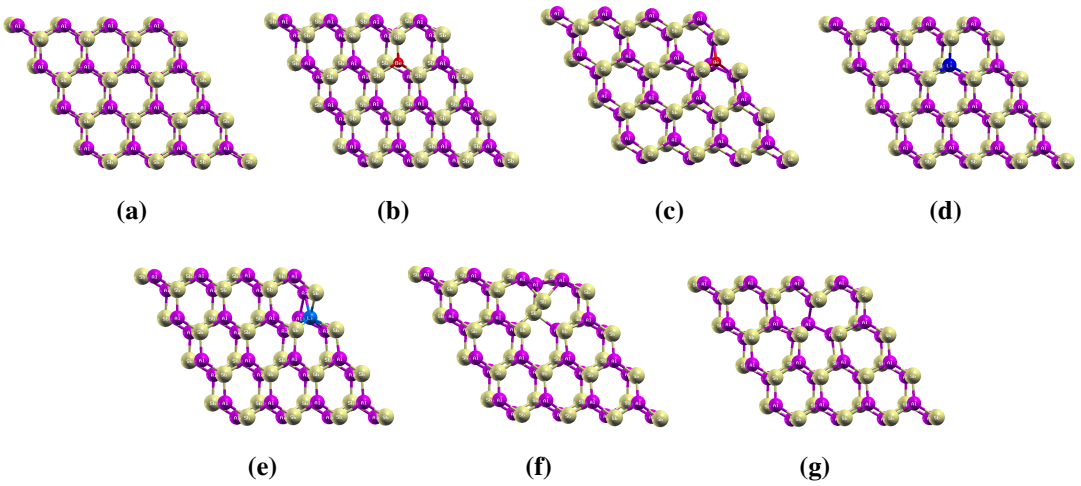

Figure 5.1: Fully relaxed geometric structures of (a) pristine; (b) Be impurity at the Al site; (c) Be impurity at the Sb site; (d) Li impurity at the Al site; (e) Li impurity at the Sb site; (f) Al vacancy and (g) Sb vacancy.

The hexagonal shape is formed between three Al atoms and three Sb atoms. To ascertain the structural properties of the pristine and defective systems, the bond distant for the unrelax and fully relaxed structures were predicted as listed in Table 5.1.

Table 5.1: The unrelax (UR) and relaxed (R) bond length in Å of atoms of defective AlSb. The relaxed pristine Al–Sb bond length (PR) is 2.686 Å.

Defect	Atoms	Unrelaxed (UR)	Relaxed (R)	UR−R	R−PR
Be_{Al}	$Be-Sb$	2.686	2.451	0.235	0.235
Be_{Sb}	$Al-Be$	2.686	2.409	0.277	0.277
Li_{Al}	$Li-Sb$	2.686	2.696	0.010	0.010
Li_{Sb}	$Al-Li$	2.686	2.989	0.303	0.303
V_{Al}	$Al-Sb$	2.686	2.686	0.000	0.000
V_{Sb}	$Al-Sb$	2.686	2.693	0.007	0.007

For the pristine supercell, the Al–Al, Sb–Sb and Al–Sb nearest neighbour bond length are 4.12, 4.12 and 2.69 Å, respectively. When Be and Li defects are introduced into the pristine supercell of AlSb, the bond distances between Be, Li and the nearest neighbour Sb (Al) atoms after structural relaxation are 2.45 (2.41) and 2.70 (2.80) Å, respectively. The difference in the bond length results from the different size of the dopants. For example, the radius of Be is smaller than the radius of the host atoms. The relaxed geometric structures show that as a result of the introduced defects, the entire systems experience strain and breaking of symmetry. Due to stress in the system, the internal energy is increased which could affect the overall strain of the system, hence leading to the distortion of the crystal arrangement. This experienced distortion affects the bond length as well as the bond angle. Due to the different radius of Be atom relatively to that of the Al and Sb atoms, the defect relaxed inward. The different radius of Li atom relatively to the Al and Sb atoms caused an inward relaxation. The bond length of the nearest neighbour Al–Sb for the vacancy (V_{Al}) and (V_{Sb}) are 0.01 and 0.27 %, respectively different from the pristine relaxed Al–Sb bond length. The amount of strain experienced by the host when defects are introduced could play a vital role in the energy of formation.

5.2 Stability and energetics of defects

To determine the stability of defects in AlSb due to the introduction of the Li and Be at the lattice sites of Al and Sb, as well as Sb and Al vacancies, the formation energy of the Be_{Al}, Be_{Sb}, Li_{Al}, Li_{Sb}, V_{Al} and V_{Sb} were calculated. The aforementioned defects are usually created via electron bombardment, sputtering and ion implantations under different irradiation conditions.

Table 5.2: The energy of formation E_{form} (eV) of vacancy and substitutional impurities in AlSb.

Defects	E_{form}
Be_{Al}	0.05
Be_{Sb}	0.30
Li_{Al}	0.27
Li_{Sb}	0.09
V_{Al}	0.45
V_{Sb}	1.26

Table 5.2 lists the formation energies of defects in AlSb. The formation energy of the Be_{Al} is lower than that of the Be_{Sb}, this indicates that under equilibrium conditions, Be is energetically more favourable when it is on the Al atomic site relative to when at the Sb atomic site. This further shows that during implantation, Be_{Al} will form with relatively lower energy compared to the Be_{Sb}. The formation energy of the Li_{Sb} is lower than that of the Li_{Al}, this shows that the Li is more stable at the Sb atomic site compared to the Al atomic site. Exploring the stability of the intrinsic vacancy, the formation energy of the V_{Al} is lower than that of the V_{Sb}. This corroborates that under equilibrium conditions, the Al vacancy is more favourable than the Sb vacancy.

This results show that Be_{Al} is the most stable defect with energy of 0.05 eV. The different formation energies of the Be_{Al}, Be_{Sb}, Li_{Al}, Li_{Sb}, V_{Al} and V_{Sb} could be attributed to the amount of the strain experienced by the systems along the xy plane.

5.3 Electronic properties

The electronic properties of defects in AlSb, i.e., the density of states (DOS) of the various relaxed structures, were plotted as displayed in Figure 5.2.

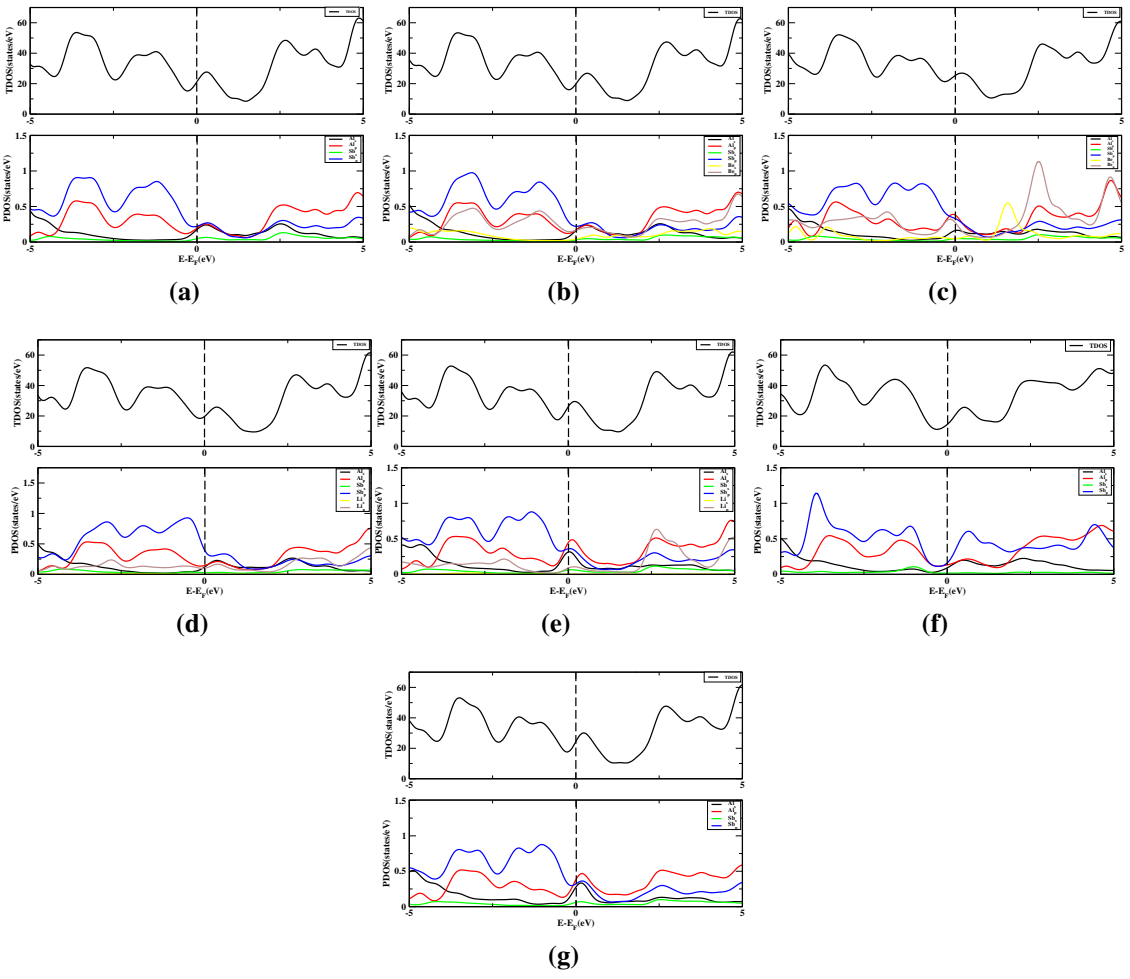

Figure 5.2: The TDOS and PDOS plots of (a) pristine; (b) Be impurity at the Al site; (c) Be impurity at the Sb site; (d) Li impurity at the Al site; (e) Li impurity at the Sb site; (f) Al vacancy and (g) Sb vacancy. The Fermi level is set to 0 eV.

The DOS of the pristine AlSb structure as shown in Figure 5.2a, has the total density of states (TDOS) on the top panel and the projected density of states (PDOS) on the bottom panel. This same procedure is adopted for other defects presented in this report. The dotted line represents the Fermi level which is set to zero eV. The PDOS plots show that the AlSb systems exhibit properties similar to a semi-metal. This is in contrasts to the experimental data. This is obvious because of the exchange correlation used in this

work. The GGA as reported in Chapter 2 have been known to wrongly predict accurately, the band gap of materials most especially semiconductor materials. The dominant states for the pristine AlSb peaks around the Fermi level are contributions from the Al and Sb p-orbitals. While for the Li_{Al}, Be_{Al} and V_{Al} systems, the dominant contribution to the states around the Fermi level are the Sb p-orbitals. According to Figure 5.2d, it is observed that in spite of the orbital hybridization, the Li_{Al} exhibit metallic behaviour. For the Li_{Sb}, the Li s-orbital is not visible at the Fermi level as shown in Figure 5.2e, however, there was strong orbital hybridization between the p-orbital of the Li atom and the Al p-orbitals as well as Sb p-orbitals. The PDOS plot for the V_{Sb} as shown in Figure 5.2g, has a dominant peak at the Fermi level, which is a contribution from all the participating orbital except the s-orbital of the Sb atoms.

CHAPTER 6

Conclusions

This chapter presents the summary of this thesis. In addition, recommendations for future work are listed.

6.1 Summary

This thesis presents the Al and Sb vacancies in 2D AlSb. The structural, electronic and formation energy of Al and Sb vacancy in AlSb were predicted. The Al vacancy has a relatively lower formation energy than the Sb vacancy. Using the GGA shows that these defects in AlSb exhibit metallic character. The second kind of defect investigated is the extrinsic Be and Li doped AlSb. The Li atom was substituted for Al and Sb. This same scenario was applied to Be doped AlSb. Be at the Al atomic site is energetically favourable than when it is at the Sb atomic site. However, for Li, it is more stable when it is at the Sb atomic site in contrast to when it is at the Al atomic site. The introduction of Li and Be impurities in AlSb, modulated the band gap of the host. The Li and Be defects in AlSb exhibit a metallic character. The results presented in this thesis, will provide insight into the experimental syntheses of these defects.

6.2 Recommendation

1. More intrinsic and extrinsic defects in 2D AlSb should be investigated.

2. Charge states should be introduced into 2D AlSb to ascertain various defect levels.

3. More Robust exchange correlation such as hybrid functional, LDA+U and GGA+U should be adopted for further studies of defective 2D AlSb.

Bibliography

[1] L. Drain, *Laser ultrasonics techniques and applications*. Routledge, 2019.

[2] R. Klein, A. Altman, R. Saballos, J. Walsh, A. Tamerius, Y. Meng, D. Puggioni, S. Jacobsen, J. Rondinelli, and D. Freedman, "High-pressure synthesis of the $BiVO_3$ perovskite," *Physical Review Materials*, vol. 3, no. 6, p. 064411, 2019.

[3] J. Cheng, C. Wang, X. Zou, and L. Liao, "Recent advances in optoelectronic devices based on 2D materials and their heterostructures," *Advanced Optical Materials*, vol. 7, no. 1, p. 1800441, 2019.

[4] M. Long, P. Wang, H. Fang, and W. Hu, "Progress, challenges, and opportunities for 2D material based photodetectors," *Advanced Functional Materials*, vol. 29, no. 19, p. 1803807, 2019.

[5] D. Singh, S. K. Gupta, and Y. Sonvane, "Structural and opto-electronic properties of 2D AlSb monolayer," in *AIP Conference Proceedings*, vol. 1731, p. 120018, AIP Publishing, 2016.

[6] K. Cheewajaroen, P. Saengkaew, S. Sanorpim, V. Yordsri, C. Thanachayanont, N. Nuntawong, and W. Rathanasakulthong, "Characterization of N-type and P-type aluminum antimonides on Si substrates for room-temperature optoelectronic devices," *Materials Science in Semiconductor Processing*, vol. 88, pp. 224–233, 2018.

[7] P. Klipstein, "III–V semiconductors for infrared detectors," *Molecular Beam Epitaxy: Materials and Device Applications*, 2019.

[8] S. Y. Son, D. Lee, J. Hur, and I. T. Kim, "Facile synthesis of aluminum-antimony alloys and their application for lithium-ion and sodium-ion storage," *Journal of Nanoscience and Nanotechnology*, vol. 17, no. 10, pp. 7575–7578, 2017.

[9] D. Trichês, S. Souza, C. Poffo, J. De Lima, T. Grandi, and R. De Biasi, "Structural instability and photoacoustic study of AlSb prepared by mechanical alloying," *Journal of Alloys and Compounds*, vol. 505, no. 2, pp. 762–767, 2010.

[10] P. Tang, J.-H. Yuan, Y.-Q. Song, M. Xu, K.-H. Xue, and X.-S. Miao, "$BaAs_3$: A narrow gap 2D semiconductor with vacancy-induced semiconductor-metal transition," *ArXiv Preprint ArXiv:1904.08742*, 2019.

[11] J. Zhang, Y. Yu, P. Wang, C. Luo, X. Wu, Z. Sun, J. Wang, W. D. Hu, and G. Shen, "Characterization of atomic defects on the photoluminescence in two-dimensional materials using transmission electron microscope," *InfoMat*, vol. 1, no. 1, pp. 85–97, 2019.

[12] D. Wang, D. Han, D. West, N.-K. Chen, S.-Y. Xie, W. Q. Tian, V. Meunier, S. Zhang, and X.-B. Li, "Excitation to defect-bound band edge states in two-dimensional semiconductors and its effect on carrier transport," *NPJ Computational Materials*, vol. 5, no. 1, p. 8, 2019.

[13] M.-H. Du, "Defects in AlSb: a density functional study," *Physical Review B*, vol. 79, no. 4, p. 045207, 2009.

[14] A. Chroneos, H. A. Tahini, U. Schwingenschlögl, and R. Grimes, "Antisites in III-V semiconductors: density functional theory calculations," *Journal of Applied Physics*, vol. 116, no. 2, p. 023505, 2014.

[15] G. Rahman, S. Cho, and S. C. Hong, "Half metallic ferromagnetism of Mn doped AlSb: A first principles study," *Physica Status Solidi (B)*, vol. 244, no. 12, pp. 4435–4438, 2007.

[16] R. Mortimer, *Physical Chemistry*. Elsevier Science, 2008.

[17] D. B. Jochym, *Development of non-local density functional methods*. PhD thesis, Durham University, 2008.

[18] E. Schrödinger, "Quantization as a problem of proper values. part IV," *Annalen der Physik*, vol. 81, p. 109, 1926.

[19] M. Born and R. Oppenheimer, "Zur quantentheorie der molekeln," *Annalen der physik*, vol. 389, no. 20, pp. 457–484, 1927.

[20] U. Nwankwo, *Development of a correction term for the kinetic energy density functional*. PhD thesis, African University of Science and Technology, 2014.

[21] N. Y. Dzade, *Computational study of the interactions of small molecules with the surfaces of iron-bearing minerals*. PhD thesis, University College London, 2014.

[22] A. Szabo and N. S. Ostlund, *Modern quantum chemistry: introduction to advanced electronic structure theory*. Courier Corporation, 2012.

[23] D. R. Hartree, "The wave mechanics of an atom with a non-coulomb central field. Part I. theory and methods," in *Mathematical Proceedings of the Cambridge Philosophical Society*, vol. 24, pp. 89–110, Cambridge University Press, 1928.

[24] V. Fock, "Näherungsmethode zur lösung des quantenmechanischen mehrkörperproblems," *Zeitschrift für Physik*, vol. 61, no. 1-2, pp. 126–148, 1930.

[25] J. C. Slater, "A simplification of the Hartree-Fock method," *Physical Review*, vol. 81, no. 3, p. 385, 1951.

[26] D. P. Taylor, W. P. Hess, and M. I. McCarthy, "Structure and energetics of the water/NaCl (100) interface," *The Journal of Physical Chemistry B*, vol. 101, no. 38, pp. 7455–7463, 1997.

[27] P. Baranek, G. Pinarello, C. Pisani, and R. Dovesi, "Ab initio study of the cation vacancy at the surface and in bulk MgO," *Physical Chemistry Chemical Physics*, vol. 2, no. 17, pp. 3893–3901, 2000.

[28] S. Casassa, A. M. Ferrari, M. Busso, and C. Pisani, "Structural, magnetic, and electronic properties of the NiO monolayer epitaxially grown on the (001) Ag surface: an ab initio density functional study," *The Journal of Physical Chemistry B*, vol. 106, no. 50, pp. 12978–12985, 2002.

[29] P.-O. Löwdin, "Correlation problem in many-electron quantum mechanics I. review of different approaches and discussion of some current ideas," *Advances in Chemical Physics*, pp. 207–322, 1958.

[30] P. Hohenberg and W. Kohn, "Inhomogeneous electron gas," *Physical Review*, vol. 136, no. 3B, p. B864, 1964.

[31] W. Kohn and L. J. Sham, "Self-consistent equations including exchange and correlation effects," *Physical Review*, vol. 140, no. 4A, p. A1133, 1965.

[32] R. M. Martin, *Electronic structure: basic theory and practical methods*. Cambridge University Press, 2004.

[33] W. Kohn, A. D. Becke, and R. G. Parr, "Density functional theory of electronic structure," *The Journal of Physical Chemistry*, vol. 100, no. 31, pp. 12974–12980, 1996.

[34] J. P. Perdew, K. Burke, and M. Ernzerhof, "Generalized gradient approximation made simple," *Physical Review Letters*, vol. 77, no. 18, p. 3865, 1996.

[35] O. Bengone, M. Alouani, P. Blöchl, and J. Hugel, "Implementation of the projector augmented-wave LDA+U method: application to the electronic structure of NiO," *Physical Review B*, vol. 62, no. 24, p. 16392, 2000.

[36] M. Petersen, J. Hafner, and M. Marsman, "Structural, electronic and magnetic properties of Gd investigated by DFT+U methods: bulk, clean and H-covered (0001) surfaces," *Journal of Physics: Condensed Matter*, vol. 18, no. 30, p. 7021, 2006.

[37] P. Deák, B. Aradi, T. Frauenheim, E. Janzén, and A. Gali, "Accurate defect levels obtained from the HSE06 range-separated hybrid functional," *Physical Review B*, vol. 81, no. 15, p. 153203, 2010.

[38] A. D. Becke, "A new mixing of Hartree–Fock and local density-functional theories," *The Journal of Chemical Physics*, vol. 98, no. 2, pp. 1372–1377, 1993.

[39] A. D. Becke, "Density-functional exchange-energy approximation with correct asymptotic behavior," *Physical Review A*, vol. 38, no. 6, p. 3098, 1988.

[40] D. Hamann, M. Schlüter, and C. Chiang, "Norm-conserving pseudopotentials," *Physical Review Letters*, vol. 43, no. 20, p. 1494, 1979.

[41] G. Kresse and D. Joubert, "From ultrasoft pseudopotentials to the projector augmented-wave method," *Physical Review B*, vol. 59, no. 3, p. 1758, 1999.

[42] D. Vanderbilt, "Soft self-consistent pseudopotentials in a generalized eigenvalue formalism," *Physical Review B*, vol. 41, no. 11, p. 7892, 1990.

[43] P. E. Blöchl, "Projector augmented-wave method," *Physical Review B*, vol. 50, no. 24, p. 17953, 1994.

[44] G. Kresse and J. Furthmüller, "Efficient iterative schemes for ab initio total-energy calculations using a plane-wave basis set," *Physical Review B*, vol. 54, no. 16, p. 11169, 1996.

[45] H. Hellmann, "Einfuhrung in die quantumchemie leipzig," *Franz Deutsche*, 1937.

[46] R. P. Feynman, "Forces in molecules," *Physical Review*, vol. 56, no. 4, p. 340, 1939.

[47] E. Igumbor, *Hybrid functional study of point defects in germanium*. PhD thesis, University of Pretoria, 2017.

[48] C. Pickard and M. Payne, "Extrapolative approaches to brillouin-zone integration," *Physical Review B*, vol. 59, no. 7, p. 4685, 1999.

[49] W. D. Callister, D. G. Rethwisch, R. Hummel, and J. Newell, *Materials Science and Engineering: an introduction*. Wiley New York, 2018.

[50] E. P. DeGarmo, J. T. Black, R. A. Kohser, and B. E. Klamecki, *Materials and process in manufacturing*. Prentice Hall Upper Saddle River, 1997.

[51] W. D. Callister and D. G. Rethwisch, *Materials Science and Engineering: an introduction*. Wiley New York, 2005.

[52] S. Takeda, M. Kohyama, and K. Ibe, "Interstitial defects on $\{113\}$ in Si and Ge line defect configuration incorporated with a self-interstitial atom chain," *Philosophical Magazine A*, vol. 70, no. 2, pp. 287–312, 1994.

[53] A. Fazzio, A. Janotti, A. J. da Silva, and R. Mota, "Microscopic picture of the single vacancy in germanium," *Physical Review B*, vol. 61, no. 4, p. R2401, 2000.

[54] G. D. Watkins, "Intrinsic defects in silicon," *Materials Science in Semiconductor Processing*, vol. 3, no. 4, pp. 227–235, 2000.

[55] C. Dreyer and C. Van de Walle, "Point defects and impurities in III-nitride bulk and thin film heterostructures," *Elsevier*, 2016.

[56] F. Wang, Y. Jia, S.-F. Li, and Q. Sun, "First-principles calculation of the 6.1 å family bowing parameters and band offsets," *Journal of Applied Physics*, vol. 105, no. 4, p. 043101, 2009.

[57] A. N. Andriotis and M. Menon, "Band gap engineering via doping: a predictive approach," *Journal of Applied Physics*, vol. 117, no. 12, p. 125708, 2015.

[58] M. A. Flores, W. Orellana, and E. Menéndez-Proupin, "First-principles DFT+ GW study of oxygen-doped CdTe," *Physical Review B*, vol. 93, no. 18, p. 184103, 2016.

[59] Diwaker and A. Kumar, "A DFT study of structural and electronic properties of $Zn_{1-x}Sb_xTe$ with x = (0.25, 0.50, 0.75)," *International Journal of Modern Physics B*, vol. 31, no. 1, p. 1650249, 2017.

[60] M. L. Colussi, R. J. Baierle, and R. H. Miwa, "Doping effects of C, Si and Ge in wurtzite [0001] GaN, AlN, and InN nanowires," *Journal of Applied Physics*, vol. 110, no. 3, p. 033709, 2011.

[61] D. Demchenko, B. Earles, H. Liu, V. Avrutin, N. Izyumskaya, Ü. Özgür, and H. Morkoç, "Impurity complexes and conductivity of Ga-doped ZnO," *Physical Review B*, vol. 84, no. 7, p. 075201, 2011.

[62] S. Fan, X. Huang, and G. Gao, "Density functional theory study on electronic structures and magnetism for nitrogen-doped ZnS," *Journal of Superconductivity and Novel Magnetism*, vol. 31, no. 5, pp. 1443–1448, 2018.

[63] S. Chen, S. Zhou, W. Yan, Y. Chen, X. Qin, and W. Xiong, "Effect of Fe and Ti substitution doping on magnetic property of monolayer $CrSi_2$: a first-principle investigation," *Journal of Superconductivity and Novel Magnetism*, vol. 32, no. 5, pp. 1341–1346, 2019.

[64] W. Yan, S. Zhou, Q. Xie, C. Zhang, and Z. Zhang, "First principle investigation of $CrSi_2$ with doping V," in *Proceedings of 2011 International Conference on Electronic & Mechanical Engineering and Information Technology*, vol. 4, pp. 1747–1749, IEEE, 2011.

[65] P. Giannozzi, S. Baroni, N. Bonini, M. Calandra, R. Car, C. Cavazzoni, D. Ceresoli, G. L. Chiarotti, M. Cococcioni, I. Dabo, *et al.*, "QUANTUM ESPRESSO: a modular and open-source software project for quantum simulations of materials," *Journal of Physics: Condensed Matter*, vol. 21, no. 39, p. 395502, 2009.

[66] H. J. Monkhorst and J. D. Pack, "Special points for Brillouin-zone integrations," *Physical Review B*, vol. 13, no. 12, p. 5188, 1976.